Inorganic Chemistry
Article

Inorg. Chem. **2009**, *48*, 10239–10248 **10239**
DOI: 10.1021/ic901264e

Structural Investigation of Lanthanoid Coordination: a Combined XANES and Molecular Dynamics Study

Paola D'Angelo,*,† Andrea Zitolo,† Valentina Migliorati,† Giordano Mancini,‡ Ingmar Persson,§ and Giovanni Chillemi*,‡

†*Department of Chemistry, University of Rome "La Sapienza", P. le A. Moro 5, 00185 Roma, Italy,* ‡*CASPUR, Inter-University Consortium for Supercomputing in Research, via dei Tizii 6b, 00185 Roma, Italy, and* §*Department of Chemistry, Swedish University of Agricultural Sciences, P.O. Box 7015, SE-750 07 Uppsala, Sweden*

Received July 1, 2009

This is the first systematic study exploring the potentiality of the X-ray absorption near edge structure (XANES) technique as a structural tool for systems containing lanthanoid(III) ions. A quantitative analysis of the XANES spectra at the K- and L_3-edges has been carried out for three hydrated lanthanoid(III) ions, namely, Yb, Nd, and Gd, in aqueous solution and in the isostructural trifluoromethanesulfonate salts. The structural and dynamic properties of the hydrated lanthanoid(III) ions in aqueous solution have been investigated by a combined experimental-theoretical approach employing X-ray absorption spectroscopy and molecular dynamics (MD) simulations. This method allows one to perform a quantitative analysis of the XANES spectra of ionic solutions using a proper description of the thermal and structural fluctuations. XANES spectra have been computed starting from the MD trajectory, without carrying out any minimization in the structural parameter space. A comparative K- and L_3-edge XANES data analysis is presented, demonstrating the clear advantages of the L_3-edge XANES analysis over the K-edge studies for structural investigations of lanthanoid compounds. The second hydration shells provide a detectable contribution to the L_3-edge spectra while the K-edge data are insensitive to the more distant coordination spheres because of the strong damping and broadening of the signal caused by the extremely large core hole widths. The XANES technique has been found to be a new valuable tool for the structural characterization of metal complexes both in the solid and in the liquid state, especially in the presence of low symmetry.

1. Introduction

Recently, there has been growing interest in lanthanoids and their derivatives because of the emergence of novel application fields. Apart from the well-known importance as contrast agents in magnetic resonance imaging techniques for medical diagnosis, there is a plethora of additional applications ranging from catalysis and organic synthesis, to nuclear waste management and liquid−liquid extraction from aqueous solutions. [1] Despite its importance, the fundamental understanding of the lanthanoid chemistry is still at an early stage of knowledge, as compared to 3d-transition metals. Lanthanoid cations belong to a chemical series whose hydration properties are of particular interest for both fundamental and applicative reasons, and questions about the change of structure of the first shell polyedron across the series are still at the center of recent research works. [2−5]

X-ray diffraction, [6] neutron scattering,[7,8] and extended X-ray absorption fine structure (EXAFS) [3,9,10] have been extensively used in the past to gain structural information on lanthanoid complexes both in solid state and in solution. From a computational point of view, Molecular Dynamics (MD) simulations, using classical, ab initio, or mixed quantum/classical interaction potentials have been used to determine structural and dynamical properties of

*To whom correspondence should be addressed. E-mail: p.dangelo@caspur.it (P.D.), chillemi@caspur.it (G.C.). Fax: +39-06-49913751.

(1) Floris, F. M.; Tani, A. *J. Chem. Phys.* **2001**, *115*, 4750–4765.
(2) Helm, L.; Merbach, A. E. *Eur. J. Solid State Inorg. Chem.* **1991**, *28*, 245–250.
(3) Persson, I.; D'Angelo, P.; De Panfilis, S.; Sandström, M.; Eriksson, L. *Chem.—Eur. J.* **2008**, *14*, 3056–3066.
(4) Duvail, M.; Souaille, M.; Spezia, R.; Cartailler, T.; Vitorge, P. *J. Chem. Phys.* **2007**, *127*, 034503/1–034503/11.
(5) Duvail, M.; Spezia, R.; Vitorge, P. *ChemPhysChem* **2008**, *9*, 693–696.
(6) (a) Habenschuss, A.; Spedding, F. H. *J. Chem. Phys.* **1979**, *70*, 3758–3763. (b) Habenschuss, A.; Spedding, F. H. *J. Chem. Phys.* **1980**, *73*, 442–450.
(7) Cossy, C.; Barnes, A. C.; Enderby, J. E.; Merbach, A. E. *J. Chem. Phys.* **1989**, *90*, 3254–3260.
(8) Helm, L.; Merbach, A. E. *Eur. J. Solid State Inorg. Chem.* **1991**, *28*, 245–250.
(9) Yamaguchi, T.; Nomura, M.; Wakita, H.; Ohtaki, H. *J. Chem. Phys.* **1998**, *89*, 5153–5159.
(10) D'Angelo, P.; De Panfilis, S.; Filipponi, A.; Persson, I. *Chem.—Eur. J.* **2008**, *14*, 3045–3055.

Published on Web 09/29/2009

lanthanoid(III) ions.[1,4,5,11−23] Even if the determination of the coordination geometry of lanthanoid(III) ions is quite straightforward for crystalline samples with high symmetry, [24−26] the characterization of structures in solutions and in solids where the lanthanoid(III) ions display water-deficit is more elusive and very difficult to be obtained from the standard experimental techniques.[3] The increasing interest in characterizing disordered systems has stimulated the development of complementary techniques and among these X-ray absorption near edge structure (XANES) is very promising because of its sensitivity to geometrical and electronic properties of the photoabsorber. In the past the lanthanoid L_3-edge X-ray absorption spectra have been most frequently used because the energy range involved (from 5 to 10 keV) is more accessible from standard synchrotron radiation sources. Moreover, the K-edges of lanthanoids cover the energy range 39 (La) to 63 (Lu) keV and because of the very short lifetime of the excited atomic state, the structural oscillations can be strongly damped. Nevertheless, a recent investigation on hydrated lanthanoid(III) ions both in aqueous solution and in solid trifluoromethanesulfonate salts has shown that the large widths of the core hole states do not appreciably reduce the potential structural information of the lanthanoid K-edge spectra. [10] In particular, because of the much wider *k*-range available, and the absence of double electron transitions, more accurate structural parameters are obtained from the analysis of K-edge than from the L_3-edge EXAFS data.

XANES has long been used in a phenomenological approach as a fingerprint of the absorbing atom coordination geometry and electronic state. In the past decade many codes have been developed aimed at simulating and extracting structural information from the near edge features. In all cases, calculations need a starting model for the structure and the electronic configuration of the compound under investigation, and in the case of ionic solutions the XANES spectra cannot be computed reducing the system to a single structure since the contribution from molecules and arrangements instantaneously distorted has to be properly accounted for.[27] A powerful method to analyze XANES spectra of liquids starting from the microscopic description derived from MD simulations has been recently applied to the investigation of several aqueous ionic solutions.[28−31] This methodology is very effective as it allows one to account for solvent effects in the calculation of the atomic potentials, and to include disorder effects due to the residence time of the ligands in the ion first coordination sphere and to the dynamic distortions of the coordination shells. While the quantitative XANES analysis has been successfully applied to the study of several transition metal ions in aqueous solution allowing a quantitative extraction of the relevant geometrical information about the absorbing site,[27,28,30−34] understanding and interpreting the X-ray edge-features of lanthanoids is still a methodological and theoretical challenge. The aim of the present work is to explore the potential of XANES spectroscopy as a tool to obtain accurate structural information on the coordination geometry of lanthanoid(III) ions both in solution and in the solid state, especially for complexes with low symmetry. To this end we have applied MXAN (Minuit XANes),[35] a XANES fitting routine, to the analysis of both the K- and L_3-edge spectra of some lanthanoid(III) ions in aqueous solution and of three solid aqualanthanoid trifluoromethanesulfonates $[Ln(H_2O)_n](CF_3SO_3)_3$, Ln = Nd, Gd, and Yb, and n = 9.0, 9.0 and 8.7, respectively. Comparison of the K- and L_3-edge XANES spectra of solid lanthanoid salts allowed the sensitivity toward more distant shells to be assessed. Moreover, for the first time, the quantitative XANES analysis of lanthanoid aqueous solutions has been carried out starting from MD calculations.

This work paves the way for future applications of the XANES technique for the structural characterization of lanthanoid compounds both in the solid state and in solution.

The outline of the remainder of the text is as follows. We first give details on the experimental measurements (section 2.1) and on the MD simulations (section 2.2). The validity of the structural results obtained from the simulation is then assessed by comparison with the EXAFS experimental data (section 2.3). In sections 2.4 and 2.5 we describe the XANES data analysis for solid samples and aqueous solutions, respectively. The results of the XANES analysis for the lanthanoid crystals and the combined MD-XANES

(11) Meier, W.; Bopp, P.; Probst, M. M.; Spohr, E.; Lin, J. L. *J. Phys. Chem.* **1990**, *94*, 4672–4682.
(12) Galera, S.; Lluch, J. M.; Oliva, A.; Bertran, J.; Foglia, F.; Helm, L.; Merbach, A. E. *J. Phys. Chem.* **1993**, *17*, 773–779.
(13) Helm, L.; Foglia, F.; Kowall, T.; Merbach, A. E. *J. Phys.: Condens. Matter* **1994**, *6*, A137–140.
(14) (a) Kowall, T.; Foglia, F.; Helm, L.; Merbach, A. E. *J. Phys. Chem.* **1995**, *99*, 13078–13087. (b) Kowall, T.; Foglia, F.; Helm, L.; Merbach, A. E. *J. Am. Chem. Soc.* **1995**, *117*, 3790–3799.
(15) Chaussedent, S.; Monteil, A. *J. Chem. Phys.* **1996**, *105*, 6532–6537.
(16) Kowall, T.; Foglia, F.; Helm, L.; Merbach, A. E. *Chem.—Eur. J.* **1996**, *2*, 285–294.
(17) Kim, H. S. *Chem. Phys. Lett.* **2000**, *330*, 570–576.
(18) Chaumont, A.; Wipff, G. *Inorg. Chem.* **2004**, *43*, 5891–5901.
(19) Ikeda, T.; Hirata, M.; Kimura, T. *J. Chem. Phys.* **2005**, *122*, 244507/1–244507/5.
(20) Clavaguéra, C.; Pollet, R.; Soudan, J. M.; Brenner, V.; Dognon, J. P. *J. Phys. Chem. B* **2005**, *109*, 7614–7616.
(21) Hughes, S. R.; Nguyen, T.-N.; Capobianco, J. A.; Peslherbe, G. H. *Int. J. Mass. Spectrom.* **2005**, *241*, 283–294.
(22) Clavaguéra, C.; Calvo, F.; Dognon, J. P. *J. Chem. Phys.* **2006**, *124*, 074505/1–074505/8.
(23) Ruas, A.; Guilbaud, P.; Den Auwer, C.; Moulin, C.; Simonin, J. P.; Turq, P.; Moisy, P. *J. Phys. Chem. A* **2006**, *110*, 11770–11779.
(24) Chatterjee, A.; Maslen, E. N.; Watson, K. J. *Acta Crystallogr., Sect. B* **1988**, *44*, 381–386.
(25) Santos, C. O. P.; Castellano, E. E.; Machado, L. C.; Vicentini, G. *Inorg. Chim. Acta* **1985**, *110*, 83–86.
(26) Abbasi, A.; Lindqvist-Reis, P.; Eriksson, L.; Sandström, D.; Lidin, S.; Persson, I.; Sandström, M. *Chem.—Eur. J.* **2005**, *11*, 4065–4077.
(27) D'Angelo, P.; Benfatto, M.; Della Longa, S.; Pavel, N. V. *Phys. Rev. B* **2002**, *66*, 064209/1–064209/7.
(28) D'Angelo, P.; Roscioni, O. M.; Chillemi, G.; Della Longa, S.; Benfatto, M. *J. Am. Chem. Soc.* **2006**, *128*, 1853–1858.
(29) (a) Merkling, P. J.; Muñoz-Páez, A.; Martínez, J. M.; Pappalardo, R. R.; Sánchez Marcos, E. *Phys. Rev. B* **2001**, *64*, 092201/1–092201/4. (b) Merkling, P. J.; Muñoz-Páez, A.; Sánchez Marcos, E. *J. Am. Chem. Soc.* **2002**, *124*, 10911–10920. (c) Carrera, F.; Torrico, F.; Richens, D. T.; Muñoz-Páez, A.; Martķnez, J. M.; Pappalardo, R. R.; Sánchez Marcos, E. *J. Phys. Chem. B* **2007**, *111*, 8223–8233.
(30) D'Angelo, P.; Migliorati, V.; Mancini, G.; Chillemi, G. *J. Phys. Chem. A* **2008**, *112*, 11833–11841.
(31) D'Angelo, P.; Migliorati, V.; Mancini, G.; Barone, V.; Chillemi, G. *J. Chem. Phys.* **2008**, *128*, 84502–84508.
(32) Chillemi, G.; Mancini, G.; Sanna, N.; Barone, V.; Della Longa, S.; Benfatto, M.; Pavel, N. V.; D'Angelo, P. *J. Am. Chem. Soc.* **2007**, *129*, 5430–5436.
(33) D'Angelo, P.; Benfatto, M. *J. Phys. Chem. A* **2004**, *108*, 4505–4514.
(34) Frank, P.; Benfatto, M.; Szilagyi, R.; D'Angelo, P.; Della Longa, S.; Hodgson, K. O. *Inorg. Chem.* **2005**, *44*, 1922–1933.
(35) Benfatto, M.; Della Longa, S. *J. Synchrotron Radiat.* **2001**, *8*, 1087–1094.

approach for aqueous solutions are given in section 3, showing the difference in cluster size dependence between the K- and L_3-edge spectra for the Yb, Gd and Nd trications. Section 4 summarizes and concludes.

2. Experimental Section

2.1. X-ray Absorption Measurements. Aqueous solutions of the lanthanoid(III) ions (Ln(III)) were made by dissolving a weighed amount of hydrated trifluoromethanesulfonates $[Ln(H_2O)_n](CF_3SO_3)_3$ (in which Ln = Nd, Gd, and Yb) in freshly distilled water. The concentration of the samples was 0.2 M, and the solutions were acidified to about pH = 1 by adding trifluoromethanesulforic acid to avoid hydrolysis. Solid $[Nd(H_2O)_9](CF_3SO_3)_3$, $[Gd(H_2O)_9]$ $(CF_3SO_3)_3$, and $[Yb(H_2O)_{8.7}](CF_3SO_3)_3$ were diluted with boron nitride to give an absorption change over the edge of about one logarithmic unit. The K-edge spectra were collected at ESRF, on the bending magnet X-ray-absorption spectroscopy beamline BM29, [36] in transmission geometry. The storage ring was operating in 16-bunch mode with a typical current of 80 mA after refill. The aqueous solutions were kept in cells with Kapton film windows and Teflon spacers ranging from 2 to 3 cm depending on the sample. The L_3-edge measurements were performed at the wiggler beamline 4−1 at the Stanford Synchrotron Radiation Laboratory (SSRL), Stanford, U.S.A., which was operated at 3.0 GeV and a maximum current of 100 mA. In this case simultaneous data collection was performed both in transmission and fluorescence mode. The stations at ESRF and SSRL were equipped with a Si[511] and Si[111] double-crystal monochromator, respectively. Higher order harmonics were reduced by detuning the second monochromator crystal to reflect, at the end of the scans, 80% of maximum intensity at the K-edge energies and 30−50% of maximum intensity at the L_3-edges, with the lower value at lower energy. Internal energy calibration was made when possible with a foil of the corresponding lanthanoid metal.

2.2. MD Simulations. MD simulations of Nd(III), Gd(III), and Yb(III) ions in aqueous solution have been performed using the ab initio effective two-body potentials developed by Floris et al.[1], obtained by fitting the parameters of a suitable analytical function on an ab initio potential energy surface. The SPC/E water intramolecular potential was used in the fitting procedure.[37] Three uncharged massless interaction sites were added to the water molecule: two of these (L_1 and L_2) are symmetrically located on the axis going through the O atom, perpendicular to the water molecular plane; the third virtual site (L_3) is on the C_2 axis on the opposite side with respect to the hydrogen atoms. A thorough description of the procedure used to obtain the ab initio potential energy function can be found in ref 1. The potential functions have the following analytical form:

$$U_{\mathrm{Mi}}(r) = U_{\mathrm{Coul}} + A_i r_{Mi}^{-4} + B_i r_{Mi}^{-6} + C_i r_{Mi}^{-8} + D_i r_{Mi}^{-12} + F_i e^{-G_i r_{Mi}} \quad (1)$$

where U_{Coul} is the Coulomb interaction computed with atomic charges as in the SPC/E model;[37] M stands for one of three lanthanoid ions and i is an interaction site on water, that is, the water oxygen and hydrogen atoms and the three dummy atoms and r_{Mi} is the ion-interaction site distance. A_i,..., G_i are the potential function parameters obtained by the fitting procedure (see Table 2 of ref 1). The simulated systems were composed by one Ln(III) ion and 809 water molecules (for a total of 4855 atoms and virtual interaction sites) in a cubic box, using periodic boundary conditions. The box side was always 29.054 Å. All simulations were performed in a NVT ensemble at 300 K using the Berendsen method [38] with a coupling constant of 0.01 ps. A time step of 1 fs was used, saving a configuration every 25 time steps. Calculations were carried out using the GROMACS package version 3.2.1,[39] modified to include the effective pair potentials. Short-range interactions have been truncated at 9 Å and the Particle Mesh Ewald [40] method was employed to treat long-range electrostatic effects while an homogeneous background charge has been used to compensate for the presence of the Ln(III) ion.[41] MD simulations of 5 ns were used to sample each of the three systems, after an equilibration phase of 1 ns.

2.3. Structural Analysis of MD Simulations. The structural properties of the three aqueous solutions are described in terms of radial distribution functions, $g_{Ln\text{-}O}(r)$ and $g_{Ln\text{-}H}(r)$:

$$g_{AB}(r) = \frac{\langle \rho_B(r) \rangle}{\langle \rho_B \rangle_{local}} = \frac{1}{N_A \langle \rho_B \rangle_{local}} \sum_{i=1}^{N_A} \sum_{j=1}^{N_B} \frac{\delta(r_{ij} - r)}{4\pi r^2} \quad (2)$$

where $\langle \rho_B(r) \rangle$ is the particle density of type B at distance r around type A, and $\langle \rho_B \rangle_{local}$ is the particle density of type B averaged over all spheres around particle A with radius r_{max}.

The Ln−O and Ln−H $g(r)$'s obtained from the MD simulations are shown in Figure 1 while the main structural results are collected in Table 1. The first peak positions of the $g(r)$'s show the expected lanthanoid contraction with an elongation of the first hydration shell going from Yb(III) to Nd(III). Inspection of Table 1 reveals that the first maximum positions of the present simulations are shorter than those obtained from Floris et al. (see Table 3 of ref 1) and are in better agreement with the experimental results. The shortening of the Ln−O first shell distance could be due to the larger box size used in our simulations which allows a better treatment of the ion−solvent interactions. However, a direct proof of the reliability of the MD simulations has been obtained by comparison with EXAFS experimental data. Recent investigations carried out on metal ion aqueous solutions have shown that the EXAFS technique can be profitably used to assess the reliability of structural results obtained from computer simulations [42,43]. Here, we have used the K-edge spectra of Ln(III) ions in aqueous solutions as it has been shown that the K-edge EXAFS data provide more accurate structural results as compared to the L_3-edge ones.[10] For disordered systems the $\chi(k)$ signal is represented by the equation:

$$\chi(k) = \int_0^\infty \mathrm{d}r\, 4\pi\rho r^2 g(r)\, A(k,r) \sin[2kr + \phi(k,r)] \quad (3)$$

where $A(k, r)$ and $\phi(k, r)$ are the amplitude and phase functions, respectively, and ρ is the density of the scattering atoms. A direct comparison between MD and EXAFS results can be performed by calculating the $\chi(k)$ theoretical signal associated with the MD Ln−O and Ln−H $g(r)$'s and by comparing it with the experimental spectrum, without carrying out any minimization procedure. The $\chi(k)$ theoretical signals have been calculated by

(36) Filipponi, A.; Borowski, M.; Bowron, D. T.; Ansell, S.; De Panfilis, S.; Di Cicco, A.; Itiè, J. P. *Rev. Sci. Instrum.* **2000**, *71*, 2422–2432.
(37) Berendsen, H. J. C.; Grigera, J. R.; Straatsma, T. P. *J. Phys. Chem.* **1987**, *91*, 6269–6271.
(38) Berendsen, H. J. C.; Postma, J. P. M.; Di Nola, A.; Haak, J. R. *J. Chem. Phys.* **1984**, *81*, 3684–3690.
(39) Berendsen, H. J. C.; van der Spool, D.; van Drunen, R. *Comput. Phys. Commun.* **1995**, *91*, 43–56.
(40) (a) Darden, T.; York, D.; Pedersen, L. *J. Chem. Phys.* **1993**, *98*, 10089–10092. (b) Essmann, U.; Perera, L.; Berkowitz, M. L.; Darden, T.; Lee, H.; Pedersen, L. *J. Chem. Phys.* **1995**, *103*, 8577–8592.
(41) Hummer, G.; Pratt, L. R.; Garcia, A. E. *J. Phys. Chem. A* **1998**, *102*, 7885–7895.
(42) D'Angelo, P.; Di Nola, A.; Filipponi, A.; Pavel, N. V.; Roccatano, D. *J. Chem. Phys.* **1994**, *100*, 985–994.
(43) D'Angelo, P.; Barone, V.; Chillemi, G.; Sanna, N.; Meyer-Klaucke, W.; Pavel, N. V. *J. Am. Chem. Soc.* **2002**, *124*, 1958–1967.

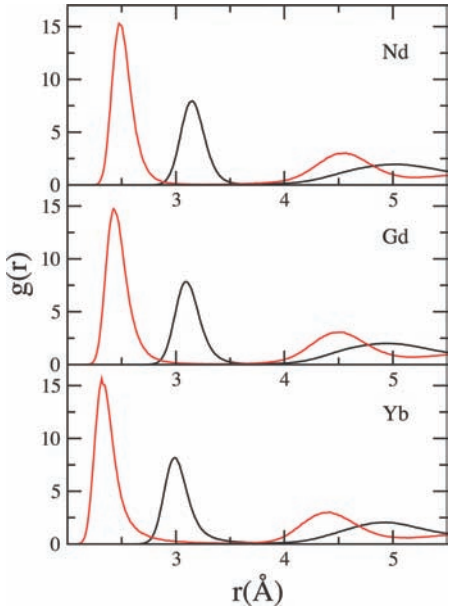

Figure 1. Ln−O (red line) and Ln−H (black line) radial distribution functions obtained for aqueous solutions of Nd(III), Gd(III), and Yb(III) from MD simulations.

Table 1. Positions (in Å) at Maxima of Ln−O and Ln−H $g(r)$'s

	Nd−O	Nd−H	Gd−O	Gd−H	Yb−O	Yb−H
			First Maxima			
Floris et al.[1]	2.53	3.18	2.46	3.10	2.37	3.02
this work	2.48	3.15	2.43	3.09	2.32	2.99
			Second Maxima			
Floris et al.[1]	4.58	5.01	4.50	4.94	4.41	4.93
this work	4.54	5.01	4.50	4.93	4.38	4.91

means of the GNXAS program, [44] and a thorough description of this procedure can be found in refs 43,45. In the analysis the S_0^2 parameter, which accounts for an overall intensity rescaling, and E_0, which aligns the experimental and theoretical energy scales, were taken from the results reported in ref 10.

In the upper panels of Figure 2 the comparison between the EXAFS experimental signal and the theoretical curves calculated using the MD $g(r)$'s is reported for the Nd(III), Gd(III), and Yb(III) ions. The first two curves from the top of each panel are the two-body Ln−O and Ln−H first shell contributions ($\gamma^{(2)}$) while the remainder of the figure shows the total theoretical contributions compared with the experimental spectra and the resulting residuals. The $\gamma^{(2)}$ signals are shown multiplied by k^2 for better visualization. As expected, the dominant contribution to the total EXAFS spectrum is given by the Ln−O first shell signal and, as a consequence, the EXAFS structural information is particularly accurate for the shape of the Ln−O $g(r)$'s first peaks, only. The Fourier transform (FT) moduli of the EXAFS $\chi(k)k^2$ theoretical, experimental, and residual signals are shown in the lower panels of Figure 2. The FT's have been calculated in the k-range 3.5−15.0 Å^{-1} with no phase shift correction applied. The FT spectra show a prominent first shell peak which is mainly due to the Ln−O first shell distance. Nevertheless, the Ln−H FT peaks are located at about 2.4 Å, giving rise to a shoulder on the first peak. Overall, the calculated EXAFS spectra match the experimental data reasonably well in all cases showing that the structural and dynamical information derived from the MD simulations is basically correct and that the SPC/E water model provides reliable values for the ion−water distances. However, in the case of the Yb(III) ion, the agreement is slightly worse, and the residual curve shows the presence of a spurious leading frequency. This small mismatch between the experimental and theoretical curves reflects the lower accuracy of the Yb(III) MD simulation, as already pointed out by Floris et al.[1]

2.4. XANES Data Analysis of Crystalline Samples. The quantitative XANES data analysis of the crystalline samples has been performed by means of the MXAN procedure which is described in detail elsewhere.[35] The X-ray absorption cross section is calculated in the framework of the full multiple-scattering scheme within the Muffin-tin approximation for the shape of the potential. The real part of the exchange term is calculated using the Hedin-Lundqvist energy-dependent potential, while the inelastic losses are accounted for by convolution with a broadening Lorentzian function having an energy-dependent width.[35]

Least-squares fits of the XANES experimental data have been performed by minimizing the R_{sq} function defined as

$$R_{sq}(\{\lambda\}) = \sum_{i=1}^{N} [\alpha_{exp}(E_i) - \alpha_{mod}(E_i;\lambda_1,\lambda_2,...,\lambda_p)]^2 \; W(E_i) \quad (4)$$

where N is the number of experimental points with energy E_i, $\{\lambda\} = (\lambda_1, \lambda_2, ..., \lambda_p)$ are the p parameters to be refined, and $W(E_i)$ is a weight function.[46]

The K-edge XANES spectra of lanthanoid(III) ions are strongly affected by the short core-hole lifetime of the excited photoelectron (the core-hole widths at the K-edges are Γ = 17.3, 22.3, and 31.9 eV for Nd, Gd, and Yb, respectively.)[47] As a consequence the edge resonance is strongly damped and the intensity of the main transition peaks becomes very small. Recently, core-hole width deconvolution methods have been developed [48] and applied to the analysis of the XANES spectra at the Hg L_3- and Cd K-edges.[31,32,49] This treatment largely facilitates the detection of spectral features and the comparison with theoretical calculations. Even if in principle the deconvolution procedure could introduce small distortions in the experimental data, the advantage of this approach is to avoid the use of the phenomenological broadening function in the calculation of the theoretical spectrum to mimic electronic damping. In the present case the Nd, Gd, and Yb K-edge raw experimental data have been deconvolved of the whole tabulated core hole width and a Gaussian filter with full width at half-maximum of about 7.4, 8.0, and 12.4 eV has been used, for Nd, Gd, and Yb, respectively. The MXAN fitting procedure has been applied to lanthanoid(III) ions in hydrated trifluoromethanesulfonate crystals including either the first shell water molecules only or the first plus the second coordination shells. The hydrogen atoms were always included in the analyses. The cluster size and the l_{max} value (i.e., the maximum l-value of the spherical harmonic expansion of the scattering path operators) were chosen on the basis of a convergence criterion. All of the non-structural parameters obtained from the minimization procedures are listed in Supporting Information, Table S1.

2.5. XANES Data Analysis of Aqueous Solutions. The XANES spectra of Ln(III) ions in aqueous solution have been analyzed starting from the microscopic description of the system derived from MD simulations. In the first step the XANES spectra

(44) Filipponi, A.; Di Cicco, A.; Natoli, C. R. *Phys. Rev. B* **1995**, *52*, 15122–15134.
(45) Burattini, E.; D'Angelo, P.; Giglio, E.; Pavel, N. V. *J. Phys. Chem.* **1991**, *95*, 7880–7886.
(46) Benfatto, M.; Della Longa, S.; Natoli, C. R. *J. Synchrotron Radiat.* **2003**, *10*, 51–57.
(47) Krause, M. O.; Oliver, J. H. *J. Phys. Chem. Ref. Data* **1979**, *8*, 329–338.
(48) Filipponi, A. *J. Phys. B: At. Mol. Opt. Phys.* **2000**, *33*, 2835–2846.
(49) Kodre, A.; Padežnik Gomilšek, J.; Mihelič, A.; Arčon, I. *Radiat. Phys. Chem.* **2006**, *75*, 188–194.

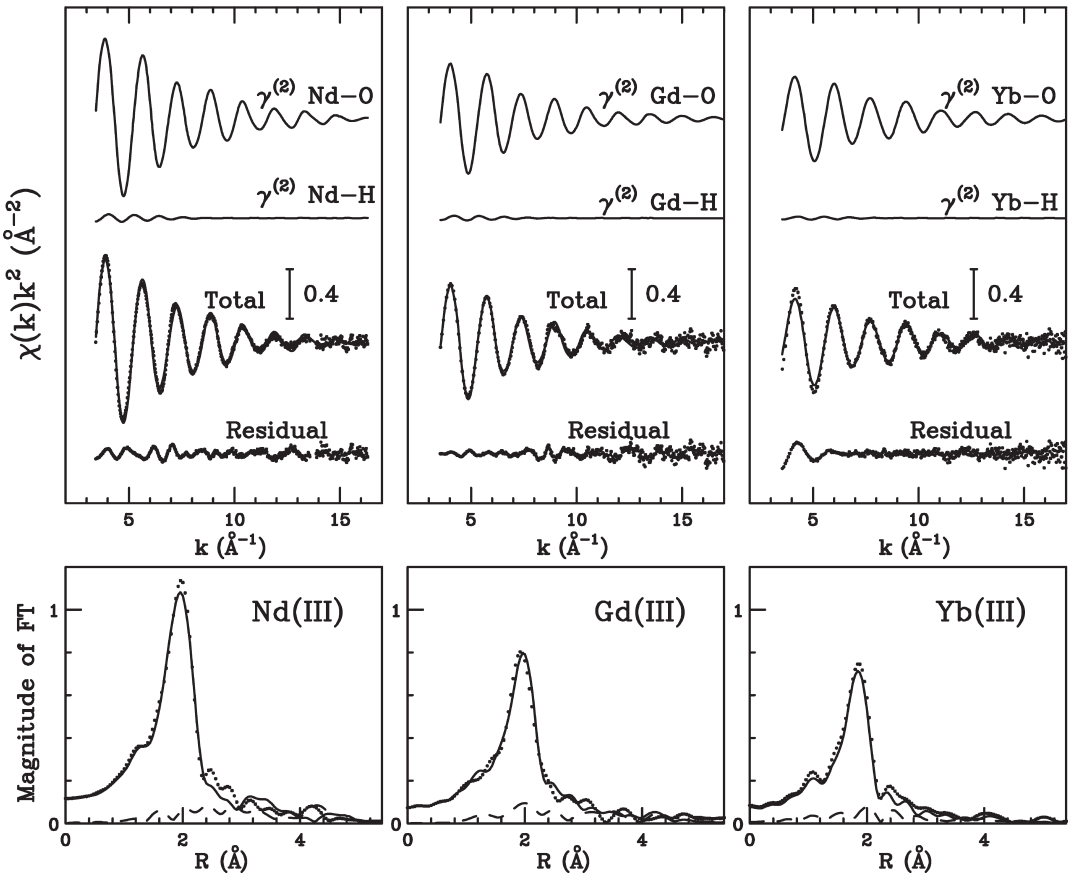

Figure 2. Analysis of the K-edge EXAFS spectra of aqueous solutions of Nd(III) (left panel), Gd(III) (middle panel), and Yb(III) (right panel) starting from the Ln−O and Ln−H radial distribution functions obtained from MD simulations. From the top to the bottom of each panel, the following curves are reported: the Ln−O first shell signals, the Ln−H first shell signals, the total theoretical signals compared with the experimental spectrum, and the residual curves. The lower panels show the non-phase-shift-corrected Fourier transforms of the experimental data (dotted line), of the total theoretical signals (full line), and of the residual curves (dashed-dotted line).

associated with the MD trajectories have been calculated using only the real part of the HL potential, that is, theoretical spectra do not account for any intrinsic and extrinsic inelastic process.

In the second step a minimization in the non-structural parameter space has been carried out to perform a comparison with the experimental data. In particular, the inelastic processes are accounted for by convolution with a broadening Lorentzian function having an energy-dependent width of the form $\Gamma(E) = \Gamma_c + \Gamma_{mfp}(E)$. The energy-dependent term $\Gamma_{mfp}(E)$ represents the intrinsic and extrinsic inelastic processes,[46] and it is zero below an energy onset E_s (which in extended systems corresponds to the plasmon excitation energy), and starts increasing from a given value A, following the universal functional form of the mean free path in solids.[50] Both the onset energy E_s and the jump A are introduced in the $\Gamma_{mfp}(E)$ function via an arctangent functional form to avoid discontinuities and are determined from a minimization procedure. All the optimized values are reported in Supporting Information, Table S1. In the case of the K-edge XANES spectra the constant part Γ_c, which accounts for the core-hole lifetime, has not been included in our calculations as it has been removed from the experimental data. For the L_3-edge spectra fixed Γ_c values of 4.60, 3.65, and 4.01 eV have been used for Yb, Nd, and Gd, respectively. In all cases the experimental resolution has been taken into account by convolution with a Gaussian function whose widths Γ_{exp} are reported in Supporting Information, Table S1.

For each ion two MD trajectories have been extracted from the total simulation, the former containing the first shell non-ahydrated cluster only, the latter containing both the first and the second hydration shells. In particular, we have considered all the water molecules separated from the ion by a distance shorter than 6.0 Å. From each trajectory we extracted 500 snapshots saved every 10 ps. Each snapshot has been used to generate the XANES spectrum associated with the corresponding instantaneous geometry, and the averaged theoretical spectrum has been obtained by summing all the spectra and dividing by the total number of MD snapshots used. The total sampling length that is necessary to have a statistically significant average has been determined performing, for each averaged theoretical spectrum, a statistical treatment of the data. In particular we have calculated a residual function defined as

$$RMS = \sqrt{\sum_i [\alpha^N(E_i) - \alpha^{N-1}(E_i)]^2} \qquad (5)$$

where $\alpha^N(E_i)$ is the theoretical spectrum averaged over N snapshots and the sum is extended over all the energy points E_i. A residual value of 10^{-4} was chosen to establish the number of spectra which are necessary to have a statistically significant average. The results of this analysis are shown in Supporting Information, Figure S1 for the L_3-edge of Yb(III) in water as an example. In this figure the RMS function is plotted against the number of averaged spectra for the first only and first plus second hydration shells. As evident from the plots a lower number of spectra is necessary in the former case, but in all cases 500 configurations are enough to reach convergence.

(50) Muller, J. E.; Jepsen, O.; Wilkins, J. W. *Solid State Commun.* **1982**, *42*, 365–372.

3. Results

To shed light on the sensitivity of the XANES technique both to the lanthanoid coordination polyhedra and to the higher distance coordination shells, it is very useful to compare the X-ray absorption spectra of aqueous solutions of Ln(III) ions with those of solid hydrates of known structure. Recently, it has been found that both in aqueous solution and in the hydrated lanthanoid trifluoromethanesulfonate salts the hydration structure of the Ln(III) ions is a tricapped trigonal prism (TTP) but across the series two of the capping water molecules become less and less strongly bound, and finally almost one on average is leaving the hydration cluster.[3]

The deconvolved K-edge spectrum of solid $[Yb(H_2O)_{8.7}](CF_3SO_3)_3$ is compared with the spectrum of the hydrated Yb(III) ion in aqueous solution in the upper panel of Figure 3. The two spectra are identical in the whole energy range suggesting that the short-range coordination of the Yb(III) ion in the two systems is the same. A different picture emerges from the comparison between the L_3-edge XANES spectra of Yb(III) in aqueous solution and solid trifluoromethanesulfonate (lower panel of Figure 3). In this case the two spectra show sizable differences both in the edge and higher energy region. In particular, both spectra have a sharp main peak followed by the structural oscillations, but the solid sample shows an additional hump at about 18 eV from the edge which is not present in the aqueous solution spectrum. To unveil the origin of this difference we have carried out a quantitative analysis of the K- and L_3-edge XANES data starting from the crystallographic structure of $[Yb(H_2O)_{8.7}](CF_3SO_3)_3$ [3] and refining the structural and non-structural parameters. Two sets of fits were carried out; in the former only the first coordination shell was included comprising six water molecules in the prism sites at the same distance and three in the capping sites with different Yb−O bond lengths. Note that the hydrogen atoms have been included in the analysis. It is important to stress that the exclusion of the hydrogen atoms from the EXAFS data analysis slightly worsens the quality of the fits but does not significantly affect the accuracy of the ion-oxygen first shell structural parameters.[10] Conversely, in the case of the XANES region, the inclusion of the hydrogen atoms has been found to be essential to correctly reproduce the experimental data, as previously observed for 3d-transition metal ions in aqueous solution.[27] In particular, it was found that neglect of the hydrogen contribution affects both the ion-oxygen distance determination and the width of the calculated shape resonance.[27]

The results of the fitting procedures applied both to the K- and L_3-edge spectra are shown in the upper panels of Figure 4, while the bond metrics are detailed in Supporting Information, Table S2. For the K-edge spectrum the agreement between the experimental and the calculated model is quite good, and the structural parameters obtained from the analysis are in fair agreement with the crystallographic determination. The non-structural parameters obtained from the refinements are listed in Supporting Information, Table S1. Conversely the agreement between the L_3-edge experimental spectrum of $[Yb(H_2O)_{8.7}](CF_3SO_3)_3$ and the theoretical curve including the first shell only is not satisfactory even if the main features of the spectrum are well accounted for. The main discrepancy between the theoretical and experimental

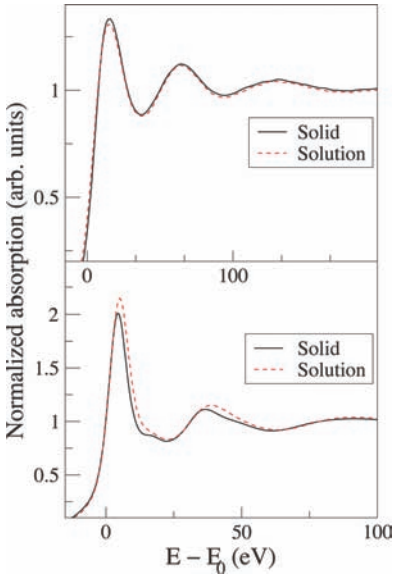

Figure 3. Upper panel: Comparison between the deconvolved K-edge XANES spectra of Yb(III) in aqueous solution (dashed red line) and solid $[Yb(H_2O)_{8.7}](CF_3SO_3)_3$ (solid black line). Lower panel: Comparison between the L_3-edge XANES spectra of Yb(III) in aqueous solution (dashed red line) and solid $[Yb(H_2O)_{8.7}](CF_3SO_3)_3$ (solid black line).

spectra is the lack of the bump at about 18 eV, and this failure of the model indicates a need to enlarge the number of atoms used in the calculation and the likelihood that the second coordination shell contributes to the XANES energy region. Therefore, we carried out a second fit including all of the atoms within a distance of 6.0 Å from the Yb(III) ion. Both the K-edge and L_3-edge fits are shown in the lower panels of Figure 4. In the case of the K-edge both the theoretical spectrum and the agreement with the experimental data are very similar to those obtained including the first shell only. As far as the L_3-edge data are concerned, the new fit shows substantial improvement in quality and the inclusion of the second shell structure leads to the appearance of the previous missing feature. The structural best fit results compare well with the crystallographic determination (Supporting Information, Table S1 and Table S2). The very good agreement between the calculated and experimental spectra gives a strong support to the reliability of the MXAN method when applied to the analysis of both the K- and L_3-edges.

Fitting procedures have been also applied to the L_3-edge XANES spectrum of the hydrated Yb(III) ion in aqueous solution using the first shell crystallographic structure of $[Yb(H_2O)_{8.7}](CF_3SO_3)_3$ as starting model.[26] The best-fit XANES spectrum is compared with the experimental data in Figure 5. In this case the agreement between the experimental and theoretical spectra is not satisfactory. This discrepancy can be due to two main reasons: the need to account for the structural disorder within the first hydration shell in the analysis of the XANES data, and the influence of the second hydration shell on the low-energy range of the absorption spectrum. Unfortunately, the effect of the high mobility of the second hydration shell does not allow construction of reliable static models including its effect. One must, therefore, resort to analysis of the XANES spectra by the microscopic description of the system derived from MD simulations.

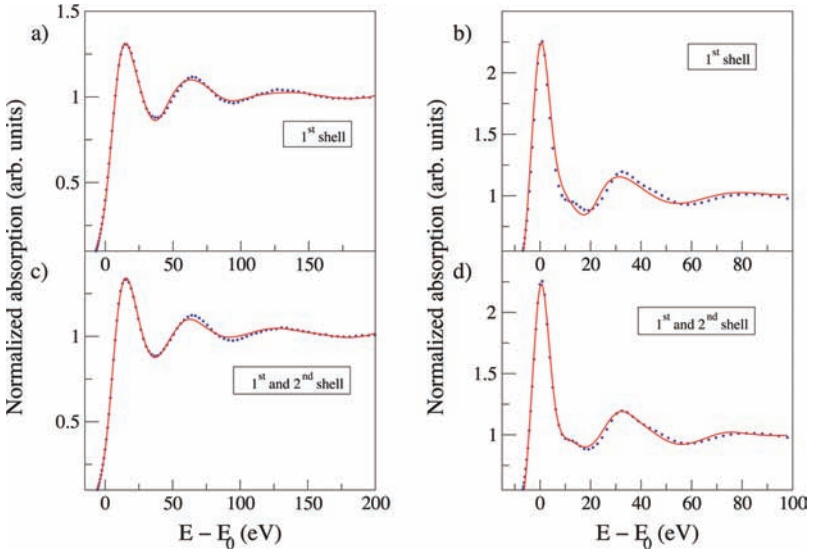

Figure 4. (a) Comparison between the deconvolved K-edge XANES experimental spectrum of solid $[Yb(H_2O)_{8.7}](CF_3SO_3)_3$ (dotted blue line) and the best-fit theoretical spectrum including only the first hydration sphere (solid red line); (b) Comparison between the L_3-edge XANES experimental spectrum of solid $[Yb(H_2O)_{8.7}](CF_3SO_3)_3$ (dotted blue line) and the best-fit theoretical spectrum including only the first hydration sphere (solid red line); (c) Comparison between the deconvolved K-edge XANES experimental spectrum of solid $[Yb(H_2O)_{8.7}](CF_3SO_3)_3$ (dotted blue line) and the best-fit theoretical spectrum including both the first and second hydration shells (solid red line); (d) Comparison between the L_3-edge XANES experimental spectrum of solid $[Yb(H_2O)_{8.7}](CF_3SO_3)_3$ (dotted blue line) and the best-fit theoretical spectrum including both the first and second hydration shells (solid red line).

3.1. XANES Analysis of Lanthanoid Aqueous Solutions from MD Simulations. As previously mentioned the quantitative XANES analysis of aqueous solutions can be carried out only if the structural disorder within the first hydration shell and the contribution of the higher distance coordination spheres are properly accounted for.[28−32] As far as the K-edge spectra are concerned, the close similarity of the solid $[Yb(H_2O)_{8.7}](CF_3SO_3)_3$ and Yb(III) aqueous solution XANES spectra (see Figure 3) suggests a substantial insensitivity toward the second coordination sphere. We have therefore decided to focus our attention on the L_3-edge spectra in water. The left panel of Figure 6 shows the averaged theoretical spectrum obtained from 500 snapshots (not including intrinsic and extrinsic inelastic process) associated with the first hydration shell of the hydrated Yb(III) ion, together with several individual instantaneous structures. The calculated XANES spectra present noticeable differences all along the energy range, showing the sensitivity of XANES to geometrical changes, and the importance of making a proper sampling of the configurational space. As far as the second shell is concerned our MD simulation suggests the presence of 27 water molecules up to about 6.0 Å from the Yb(III) ion. The XANES total theoretical spectrum obtained from 500 MD snapshots including both the first- and second-shell is shown in the right panel of Figure 6, together with several spectra computed from instantaneous configurations. In this case the individual spectra show more marked differences as compared to the first hydration shell. Considering the large deviation among instantaneous spectra it seems unlikely that a single representative configuration can be used to properly model the experimental data.

To better highlight the influence of the second hydration shell on the L_3-edge XANES spectrum of the Yb(III) ion in aqueous solution it is useful to compare the averaged spectrum calculated using first-shell-only and

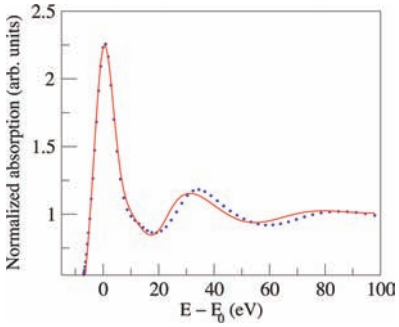

Figure 5. Comparison between the L_3-edge XANES experimental spectrum of the hydrated Yb(III) ion in aqueous solution (dotted blue line) and the theoretical best-fit spectrum calculated using a static first shell model (solid red line).

first- and second-shell clusters (see Figure 7). The calculated XANES spectra present noticeable differences in the energy range up to 50 eV from the threshold. In particular, the edge intensity is lowered in the spectrum containing only the first shell water molecules, which exhibits a different shape in the region around the first minimum. The two spectra become identical for energy values higher than 60 eV, and this finding underlines the insensitivity of the EXAFS technique toward second-shell contributions.

To assess the reliability of our results it is necessary to compare the total averaged XANES spectra with the experimental data. To this end all inelastic processes have been accounted for by convoluting the theoretical averaged spectra with a broadening Lorentzian function, and the corresponding E_s and A non-structural parameters have been optimized (see Supporting Information, Table S1). In the upper panel of Figure 8, the experimental XANES data of the Yb(III) ion in water are compared with the averaged theoretical spectrum including the first-shell clusters as derived from MD simulations.

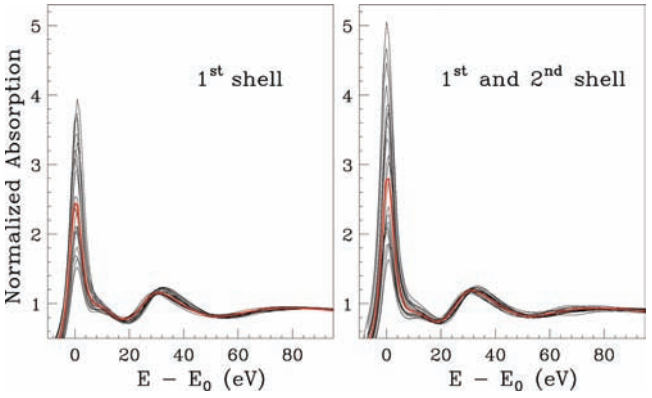

Figure 6. Left panel: Comparison of the theoretical XANES spectrum of the Yb(III) ion in water obtained from the MD average including only the first hydration shell (red line) and several spectra associated with individual MD configurations (black lines). Right panel: Comparison of the theoretical XANES spectrum of the Yb(III) ion in water obtained from the MD average including both the first and the second hydration shells (red line) and several spectra associated with individual MD configurations (black lines).

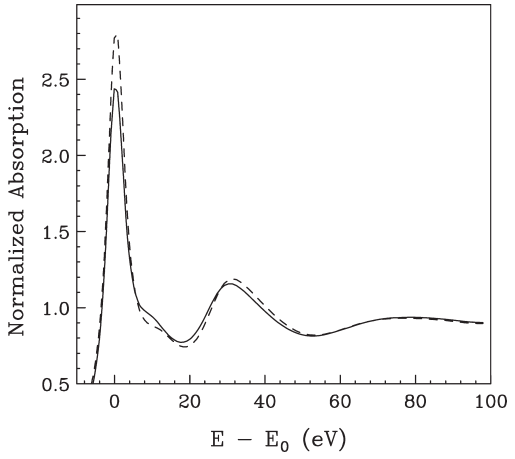

Figure 7. Comparison of the L_3-edge theoretical XANES spectrum obtained from the MD average including only the first hydration shell (solid line) and the averaged theoretical XANES spectrum including both the first and second shells (dashed line).

The overall agreement of the two spectra is not perfect in the entire energy range. In the lower panel Figure 8, the averaged theoretical spectrum including both the first and second hydration shells is compared with the experimental data. In this case, the agreement between the experimental and theoretical spectra is very good, the intensity of the white line is recovered and the shape of the first minimum region is very similar to the experimental data. It is important to remark that all the XANES spectra have been calculated using the structural information obtained from the MD simulations without carrying out any minimization in the structural parameter space. Because of the high sensitivity of the XANES technique toward the structural environment of the photoabsorber this approach is a very strict test on the quality of the potentials used in the MD simulations, and the almost perfect agreement between the averaged theoretical and experimental XANES spectra proves the reliability of the entire computational procedure.

A complete picture of the potentiality of the XANES technique for the structural characterization of

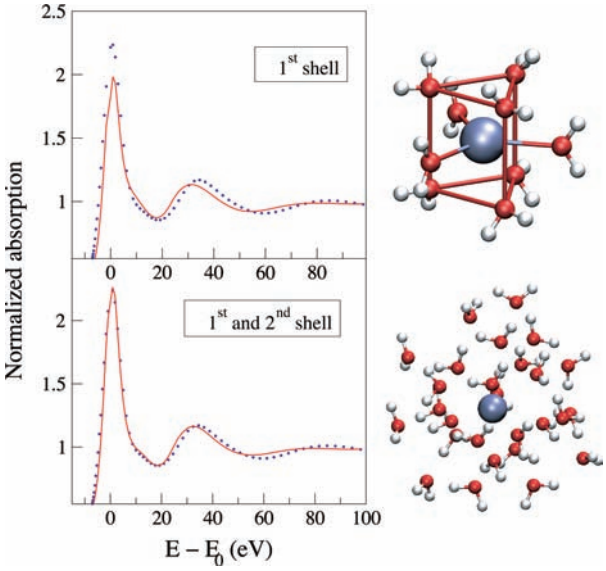

Figure 8. Upper panel: Comparison between the L_3-edge XANES experimental spectrum of Yb(III) aqueous solution (dotted blue line) and the MD averaged theoretical spectrum including only the first coordination sphere (solid red line). Lower panel: Comparison between the L_3-edge XANES experimental spectrum of the Yb(III) ion in aqueous solution (dotted blue line) and the MD averaged theoretical spectrum including both the first and the second coordination shell (solid red line).

lanthanoid solutions has been obtained by analyzing the L_3-edge XANES spectra of two additional ions, namely, Nd(III) and Gd(III). We have chosen these two additional ions as the hydration properties are known to change across the lanthanoid series. In particular, with decreasing size of the Ln(III) ion the repulsion between the first shell water molecules increases giving rise to a progressive weakening of the interaction between the central metal and the outer water molecules. As a consequence the last ions of the series show a reduced ability to structure water with a more mobile second hydration shell which becomes less observable in the XANES spectra. Also in this case it is useful to compare the XANES spectra of aqueous solutions and solid trifluoromethanesulfonates to assess the sensitivity toward the higher distance coordination shells. Figure 9 shows this comparison for the Nd(III) and Gd(III) ions. As previously observed, both the intensity of the main edge and the shape of the first minimum are not equal, and this could be due to a different flexibility of the first hydration shell and to a different coordination in the second sphere.

The analysis of the aqueous solution XANES spectra has been carried out along the line of the Yb(III) ion. Figure 10 shows the comparison between the averaged theoretical spectra computed on the basis of the MD trajectories and the experimental data. The analysis including only the first hydration shells is reported in the upper panels while the averaged theoretical spectra computed including all the water molecules up to 6 Å are shown in the lower panels. Note that for both ions the agreement between the experimental and theoretical data improves when the second hydration shell is taken into account. Also in this case the inclusion of the higher distance ligands produces additional features that are clearly detectable in the experimental data.

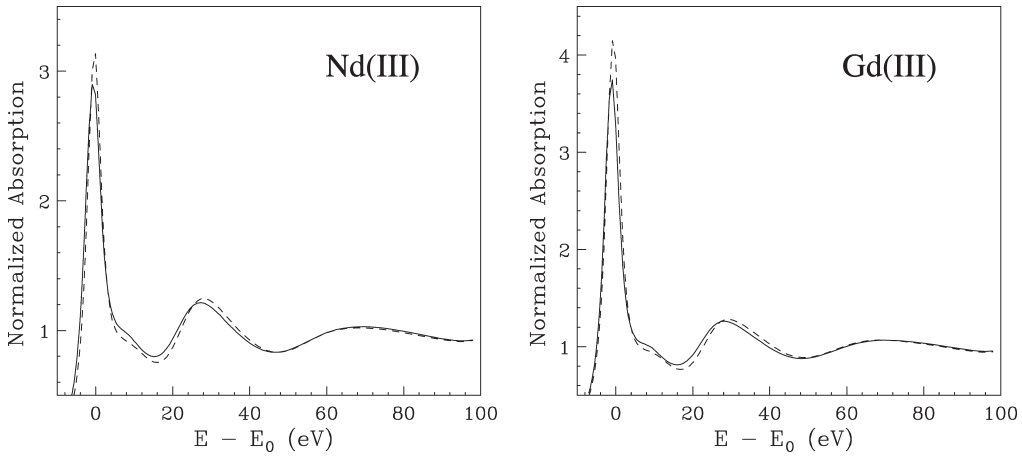

Figure 9. Left panel: Comparison between the L_3-edge XANES spectra of the Nd(III) ion in aqueous solution (solid line) and solid $[Nd(H_2O)_9](CF_3SO_3)_3$ (dashed line). Left panel: Comparison between the L_3-edge XANES spectra of the Gd(III) ion in aqueous solution (solid line) and solid $[Gd(H_2O)_9](CF_3SO_3)_3$ (dashed line).

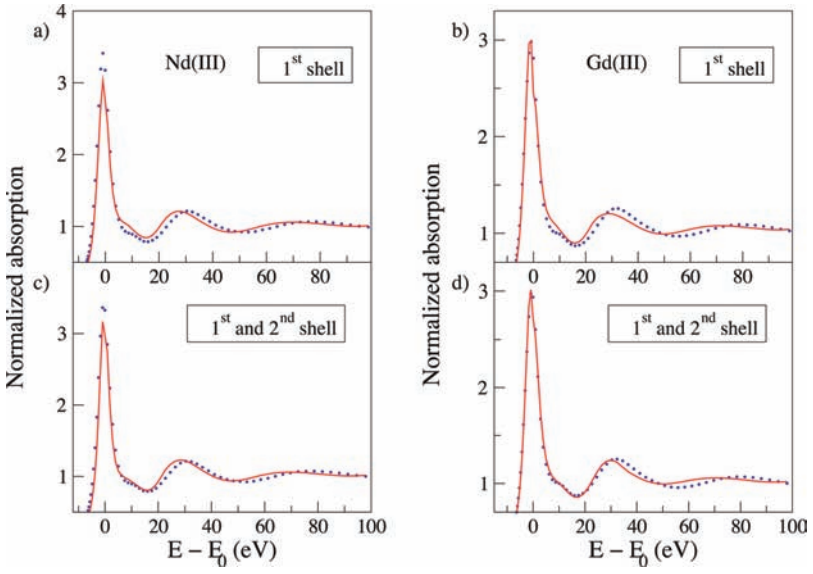

Figure 10. (a) Comparison between the L_3-edge XANES experimental spectrum of the Nd(III) ion in aqueous solution (dotted blue line) and the MD averaged theoretical spectrum including only the first hydration sphere (solid red line); (b) Comparison between the L_3-edge XANES experimental spectrum of the Gd(III) ion in aqueous solution (dotted blue line) and the MD averaged theoretical spectrum including only the first hydration sphere (solid red line); (c) Comparison between the L_3-edge XANES experimental spectrum of the Nd(III) ion in aqueous solution (dotted blue line) and the MD averaged theoretical spectrum including both the first and second hydration shells (solid red line); (d) Comparison between the L_3-edge XANES experimental spectrum of the Gd(III) ion in aqueous solution (dotted blue line) and the MD averaged theoretical spectrum including both the first and second hydration shells (solid red line).

Finally, we have used the instantaneous configurations of the MD simulations to compute K-edge averaged XANES spectra for the three ions. In this case we have included only the first shell water molecules, and the comparison with the deconvolved experimental spectra is shown in Figure 11. The agreement between the experimental and theoretical spectra is quite good for all the three ions, proving simultaneously the reliability of the procedure and the insensitivity of the K-edge XANES spectra toward higher distance coordination shells.

4. Concluding Remarks

In this paper, we have carried out, for the first time, a quantitative analysis of the K- and L_3-edge XANES spectra of Ln(III) ions in aqueous solution and solid trifluoromethanesulfonate salts which was able to highlight the potential and the limits of the XANES technique in the structural characterization of systems containing lanthanoid(III) ions. The XANES spectroscopy has been found to be a very effective probe of the geometric structure of hydrated lanthanoid clusters both in solid crystals and in aqueous solutions. For crystalline systems the XANES analysis can be profitably performed starting from a single representative structure, and this technique has been found to be more sensitive than EXAFS both to the second coordination shell and to the geometrical configuration around the absorbing atom. The analysis of the aqueous solution data has been carried out starting from the microscopic description of the systems obtained from MD simulations. Configurational averaged XANES spectra have been computed directly from the geometrical configurations generated from MD simulations. This approach, applied to the first shell cluster, allowed us to quantitatively determine the effect of disorder on the

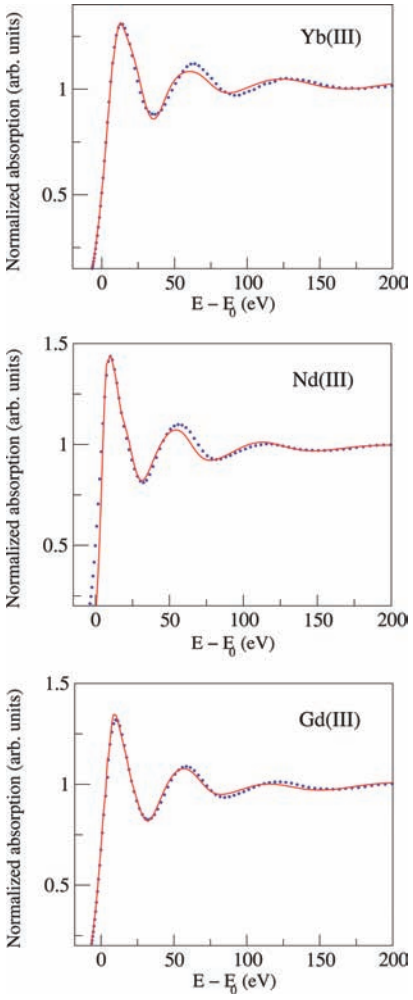

Figure 11. Comparison between the deconvolved K-edge XANES experimental spectra of the Yb(III), Nd(III), and Gd(III) ions in aqueous solution (dotted blue line) and the MD averaged theoretical spectra including only the first hydration shell (solid red line).

amplitude of the XANES spectra and to reproduce the experimental K-edge data. Conversely, a reliable reproduction of the L_3-edge experimental spectra has been obtained only by including the second shell water molecules in the calculation. L_3-edge XANES of Ln(III) ions in aqueous solutions is strongly influenced by the second hydration shell, and whereas the EXAFS data can be interpreted using a model average structure and accounting for the disorder with the Debye−Waller factor, the results presented here indicate that this approach is not applicable to the XANES region of the spectrum. Therefore, the combination of theoretical simulations and XANES is the only possible approach for the quantitative analysis of the L_3-edge XANES spectra of disordered systems.

A last remark we would like to make concerns the different sensitivity of the K- and L_3-edge XANES data. In all cases the K-edge XANES spectra have been found to be insensitive to the second coordination shell. This is due to the very short lifetime of the excited atomic state for absorption edges above 30 keV which gives rise to a strong damping and broadening of the signal. This affects in particular the high-frequency components of the measured signal and consequently reduces the sensitivity of the technique to the more distant coordination shells. In the case of the deconvolved spectra the adopted Gaussian filter has a σ value usually in the range between one-third and one-half of the core hole lifetime width. For this reason the broadening of the spectra due to the short lifetime of the excited atomic state is only partially eliminated by the deconvolution procedure. The effect is more pronounced for higher energy values of the absorption edge. As an example in the case of Yb for the deconvolved K-edge spectrum it has been used as a Gaussian filter with full width at half-maximum of 12.4 eV while the core-hole width of the L_3-edge is only 4.6 eV.

In conclusion, we show that XANES is a very profitable tool to gain direct structural information on the coordination geometry of metal complexes with low symmetry, such as the hydrated lanthanoid(III) ions, that is not achievable by other experimental techniques. The results of this investigation pave the route for the use of XANES for structural investigations of solid and liquid systems of metal ions with low symmetry.

Acknowledgment. This work was supported by CASPUR with the Standard HPC Grant 2009 entitled: "A combined X-ray absorption spectroscopy, Molecular Dynamics simulations and Quantum Mechanics calculation procedure for the structural characterization of ill-defined systems". We acknowledge the European Synchrotron Radiation Facility for provision of synchrotron radiation facilities. We would like to thank Leonardo Guetti and Calogero Natoli for helpful discussion and Michael Borowski and Simone De Panfilis for assistance in using beamline BM29. The L_3-edge data were collected at Stanford Synchrotron Radiation Lightsource (SSRL), which is a national user facility operated by Stanford University on the behalf of the U.S. Department of Energy, Office of Basic Energy Sciences. The SSRL Structural Molecular Biology Program is supported by the Department of Energy, Office of Biological and Environmental Research, and by the National Institutes of Health, National Center for Research Resources, Biomedical Technology Program. The support from the Swedish Research Council is acknowledged (I.P.).

Supporting Information Available: Figure showing the RMS function for the L_3-edge of Yb(III) in water. Listings of non-structural parameters and first shell distances obtained from the minimization procedures. This material is available free of charge via the Internet at http://pubs.acs.org.